Asymmetric cortical projections to striatal direct and indirect pathways distinctly control actions

Jason R. Klug[1,5], Xunyi Yan[1,3,5], Hilary A. Hoffman[1], Max D. Engelhardt[1], Fumitaka Osakada[2], Edward M. Callaway[2], and Xin Jin[1,3,4*]

[1] Molecular Neurobiology Laboratory, [2] Systems Neurobiology Laboratories, The Salk Institute for Biological Studies, 10010 North Torrey Pines Road, La Jolla, CA 92037, USA

[3] New Cornerstone Science Laboratory, Center for Motor Control and Disease, Key Laboratory of Brain Functional Genomics, East China Normal University, 3663 North Zhongshan Road, Shanghai 200062, China

[4] NYU–ECNU Institute of Brain and Cognitive Science, New York University Shanghai, 3663 North Zhongshan Road, Shanghai 200062, China

[5] These authors contributed equally to this work.

*Correspondence to: xjin@bio.ecnu.edu.cn

Abstract

The striatal direct and indirect pathways constitute the core for basal ganglia function in action control. Although both striatal D1- and D2-spiny projection neurons (SPNs) receive excitatory inputs from the cerebral cortex, whether or not they share inputs from the same cortical neurons, and how pathway-specific corticostriatal projections control behavior remain largely unknown. Here using a G-deleted rabies system in mice, we found that more than two-thirds of excitatory inputs to D2-SPNs also target D1-SPNs, while only one-third do so *vice versa*. Optogenetic stimulation of striatal D1- vs. D2-SPN-projecting cortical neurons differently regulate locomotion, reinforcement learning and sequence behavior, implying the functional dichotomy of pathway-specific corticostriatal subcircuits. These results reveal the partially segregated yet asymmetrically overlapping cortical projections on striatal D1- vs. D2-SPNs, and that the pathway-specific corticostriatal subcircuits distinctly control behavior. It has important implications in a wide range of neurological and psychiatric diseases affecting cortico-basal ganglia circuitry.

In Brief:

Klug, Yan et al. employed a modified rabies system in combination with slice physiology, optogenetics and behavioral tests to reveal that pathway-specific corticostriatal subcircuits distinctly control actions.

Highlights

- One-third of the excitatory inputs to D1-SPNs project to D2-SPNs, while two-third of the excitatory inputs to D2-SPNs also target D1-SPNs
- Activation of D1-SPN projecting cortical neurons triggers behavioral effects in line with postsynaptic striatal direct pathway activation
- Activation of D2-SPN projecting cortical neurons causes behavioral effects similar with co-activation of both direct and indirect pathways
- Corticostriatal subcircuits control actions in a brain-region and pathway-specific manner

Introduction

The corticostriatal circuits are critically involved in sensory, cognition, and the learning and control of actions (Aoki *et al.*, 2019; Graybiel, 1998; Haber, 2016; Hikosaka *et al.*, 1998; Jin and Costa, 2010; 2015; Kupferschmidt *et al.*, 2017; Stephenson-Jones *et al.*, 2011; Tanji, 2001; Yin and Knowlton, 2006). Dysfunctional corticostriatal circuitry has been implicated in numerous neurological and psychiatric diseases (Shepherd, 2013), including Parkinson's (Redgrave *et al.*, 2010), autism (Monteiro and Feng, 2017) and obsessive-compulsive disorder (Dalley and Robbins, 2017). The striatal direct and indirect pathways, made up of D1- vs. D2-expressing spiny projection neurons (SPNs) respectively, constitute the core components for basal ganglia functions in relation to action learning and movement control (Albin *et al.*, 1989; DeLong, 1990; Gerfen *et al.*, 1990). Numerous studies have suggested that the two pathways play distinct yet complementary role in controlling actions (Cui *et al.*, 2013; Geddes *et al.*, 2018; Hikosaka *et al.*, 2019; Hikosaka *et al.*, 2000; Jin *et al.*, 2014; Kravitz *et al.*, 2010; Markowitz *et al.*, 2018; Mink, 2003; Tecuapetla *et al.*, 2016). It is well known that D1- and D2-SPNs are spatially intermixed in the striatum and they both receive major excitatory inputs from the cerebral cortex (Bolam *et al.*, 2000; C.R. Gerfen, 2016; Pan *et al.*, 2010). Previous monosynaptic rabies tracing study has revealed that sensory and limbic cortical regions preferably send projections to D1-SPNs, compared to the motor cortical inputs biased toward D2-SPNs (Wall *et al.*, 2013). However, this anatomical analysis was based on relative percentage of various inputs to a certain population, D1 or D2, and does not reflect the absolute number of cortical projections or the crosstalk of projections to both pathways. Furthermore, how the functional distinction between these two pathways is generated in the corticostriatal circuitry, and whether the striatal D1- and D2-SPNs receive the inputs from the same or different group of cortical neurons remain

largely unknown. This is mainly due to the lack of appropriate tools to label and manipulate the specific cortical subpopulations projecting to D1- vs. D2-SPNs for functional investigations.

Here using a G-deleted rabies system in mice (Klug *et al.*, 2018; Osakada *et al.*, 2011; Wall *et al.*, 2013), we are able to selectively target and express channelrhodopsin-2 (ChR2) in presynaptic neurons projecting to D1- vs. D2-expressing SPNs. Whole-cell recordings from brain slice reveal that only one-third of the excitatory inputs to D1-SPNs target D2-SPNs, suggesting that many excitatory inputs to D1-SPNs selectively drive the direct pathway. In contrast, a large proportion of excitatory inputs to D2-SPNs send collateral projections to D1-SPNs, implying that excitatory inputs to D2-SPNs control both the indirect and direct pathways. Optogenetic stimulation of D1- vs. D2-SPN-projecting cortical neurons in vivo differently regulate locomotion, reinforcement learning and sequence behavior, in a cell-type and brain-region dependent manner. These results reveal the functional organization of cell-type- and pathway-specific corticostriatal subcircuits, and offer essential insights into how they might control behavior in health and disease.

Results

A modified rabies virus system (Klug *et al.*, 2018; Osakada *et al.*, 2011; Wall *et al.*, 2013) was employed to label and functionally target the specific cortical neurons projecting to striatal D1- versus D2-SPNs. Specifically, D1- or A2a-Cre mice (Gong *et al.*, 2007) were injected with Cre-dependent helper viruses (AAV5/EF1α-Flex-TVA-mCherry, AAV8/CA-Flex-RG) in the dorsal striatum (Klug *et al.*, 2018; Wall *et al.*, 2013) (Fig. 1A-B; see Materials and Methods). Three weeks later, either (EnvA) SAD-ΔG Rabies-GFP or (EnvA) SAD-ΔG Rabies-ChR2-mCherry was injected into the same striatal location to retrogradely infect the presynaptic

cortical neurons projecting to D1- or D2-SPNs (Fig 1B). We first injected (EnvA) SAD-ΔG Rabies-GFP in a subgroup of mice to validate the corticostriatal anatomy. In both D1- and A2a-Cre tracing experiments, intensive labeling was found in different cortical regions as expected including the midcingulate cortex (MCC) (van Heukelum *et al.*, 2020; Vogt and Paxinos, 2014) and the primary motor cortex (M1), which targets mainly the dorsal medial and dorsal lateral striatum respectively (Aoki *et al.*, 2019; Bolam *et al.*, 2000; C.R. Gerfen, 2016; Pan *et al.*, 2010; Shepherd, 2013) (Fig. 1C, D). For functional studies, (EnvA) SAD-ΔG Rabies-ChR2-mCherry was utilized to express ChR2 in the presynaptic cortical neurons projecting to D1- or D2-SPNs. To validate the functional expression of ChR2 in the cortex, whole-cell patch clamp recordings were performed from the mCherry-positive layer V pyramidal neurons in M1 around day 7 post rabies injection (Fig. 1E-G; see Materials and Methods). Both the current-voltage relationship revealed by somatic current injections (Fig. 1H) and the spiking activity elicited by blue laser frequency stimulation (Fig. 1I; Fig. S1) confirmed the overall health and the functional expression of ChR2 in the rabies-infected cortical neurons. These results thus demonstrate that we were able to successfully target and functionally express ChR2 in presynaptic cortical neurons projecting to either striatal D1- or D2-SPNs.

Taking advantage of this rabies-ChR2 system, we first sought to determine how many functional excitatory inputs that the striatal D1- and D2-SPNs might share. The possible functional organization of excitatory inputs to D1- and D2-SPNs at the single cell level, like the corticostriatal projections, could be completely segregated, totally overlapping, or partially mixed (Fig. 2A). In order to differentiate these possibilities, we made whole-cell recordings from D1- or D2-SPNs in brain slice by optogenetic stimulation of rabies-ChR2-infected excitatory terminals in striatum. We asked what the probability is that a D1- or D2-SPN targeted by the

same presynaptic excitatory inputs projecting to the nearby D1- or D2-SPN population. D1- or A2a-Cre mice were crossed to the D1- or D2-eGFP reporter line for visualizing striatal D1- vs. D2-SPNs in slice recordings (see Methods). Following the helper viruses and rabies-ChR2-mCherry injection in the D1-/A2a-Cre x D1-/D2-eGFP mice, the mCherry negative striatal SPNs were selected to be recorded in the whole-cell mode and D1- vs. D2-SPNs can be further separated based on the eGFP expression. Picrotoxin, a $GABA_A$ antagonist, was added throughout the recordings to isolate the excitatory postsynaptic currents (EPSCs). Following the blue laser stimulation of ChR2-positive presynaptic terminals in striatum, the short-latency (< 10 ms) EPSCs recorded was considered as the direct excitatory inputs on D1- or D2-SPNs (Klug *et al.*, 2018; Kress *et al.*, 2013), which can be blocked by glutamate antagonists NBQX/APV (see Methods).

Recordings from the mCherry-negative, non-starter striatal D1-SPNs in striatal D1-rabies-ChR2-infected mice revealed that with high probability (~63%) a D1-SPN receives the inputs from the presynaptic excitatory neurons projecting to surrounding D1-SPNs (Fig. 2B, D; Fig. S2). This is true from recordings in non-starter D1-SPNs identified both as mCherry (-) / eGFP (+) in D1-Cre x D1-eGFP mice and mCherry (-) / eGFP (-) in D1-Cre x D2-eGFP mice (Fig. 2B, D). Similarly, recordings from mCherry-negative non-starter striatal D2-SPNs in striatal D2-rabies-ChR2-tracing mice revealed that with a very high probability (~79%) a D2-SPN receives the inputs from the presynaptic excitatory neurons project to surrounding D2-SPNs (Fig. 2C, D; Fig. S2). Again, it is similar from recordings in non-starter D2-SPNs identified both as mCherry (-) / eGFP (+) in A2a-Cre x D2-eGFP mice and mCherry (-) / eGFP (-) in A2a-Cre x D1-eGFP mice (Fig. 2C, D). However, recordings from striatal D2-SPNs in the striatal D1-rabies-ChR2-tracing mice revealed that the chance for a D2-SPN to receive excitatory inputs

from the presynaptic neurons projecting to surrounding D1-SPNs is rather low (~40%, Fig. 2E, G; Fig. S2). In contrast, recordings from striatal D1-SPNs in the striatal D2-rabies-ChR2-tracing mice revealed that the chance for a D1-SPN to receive the excitatory inputs from the presynaptic neurons projecting to surrounding D2-SPNs is remarkably high (~73%, Fig. 2F, G; Fig. S2). These data unveil a complex picture including both parallel and crosstalk between the excitatory inputs to D1- and D2-SPNs. Notably, the likelihood that the input connectivity was significantly higher from the presynaptic excitatory inputs of D2-SPNs to D1-SPNs than from the presynaptic excitatory inputs of D1-SPNs to D2-SPNs (Fig. 2D, G). Together these results suggest largely segregated yet asymmetrically overlapping excitatory projections to striatum where the majority of excitatory inputs to D1-SPNs only target the D1-SPNs, while most excitatory inputs to D2-SPNs target both D2- and D1-SPNs.

Based on this asymmetrically overlapping functional organization, one would predict that the excitatory inputs to D1-SPNs mostly control the striatal direct pathway, while the inputs to D2-SPNs would drive both the indirect and direct pathways (Fig. 3A). To test whether this is the case, we injected rabies-ChR2-mCherry into the dorsal striatum of D1- or A2a-Cre mice as before, and implanted optic fibers bilaterally in either MCC or M1 (see Methods). This allows us to selectively activate D1- or D2-SPN projecting neurons in MCC or M1 and determine the optogenetic effects on behavior. For comparison, we performed behavioral experiments by optogenetic stimulation of striatal D1- or D2-SPNs in dorsal medial (DMS) and dorsal lateral striatum (DLS), two areas that receive dense excitatory projections from MCC and M1, respectively (Aoki *et al.*, 2019; Shepherd, 2013) (see Methods). Consistent with the previous observations (Kravitz *et al.*, 2010), optogenetic stimulation (20Hz) of D1-SPNs in the DMS or DLS facilitated locomotion (Fig. 3B, C, E, F). Conversely, optogenetic stimulation (20Hz) of

D2-SPNs in DMS significantly suppressed locomotion (Fig. 3B, D), which is less obvious in DLS (Fig. 3E, G).

Notably, high-frequency (20Hz) but not low-frequency (5Hz) optogenetic stimulation of MCC neurons that project to D1-SPNs significantly facilitated locomotion in the open field (Fig. 3H, I; Fig. S1), similar to D1-SPN activation in DMS. However, optogenetic stimulation (20Hz) of D2-SPN projecting MCC neurons in the same location did not alter locomotion in the open field (Fig. 3H, J), in contrast with the effects of stimulation of D2-SPNs in DMS (Fig. 3D). Similarly, high-frequency optogenetic stimulation (20Hz) of M1 neurons that project to D1-SPNs facilitated locomotion in the open field (Fig. 3K, L; Fig. S1), while 20Hz stimulation of the M1 neurons projecting to D2-SPNs did not significantly alter locomotion (Fig. 3K, M). Further control experiments employing the same optogenetic stimulation in the exact cortical locations but with ChR2 expression only in the striatum do not generate any behavioral phenotypes (Fig. S3). It thus rules out the possibility that the behavioral effects observed by cortical stimulation in the rabies-ChR2 mice were triggered through direct striatal activation due to the light penetration into the striatum. These results are consistent with the functional connectivity in which the excitatory inputs to D1-SPNs mostly drive the direct pathway, and the inputs to D2-SPNs target both the indirect and direct pathways (Fig. 3A). It also suggests that the cortical neurons in the same cortical layer and spatial location could differently control actions depending on their striatal projection targets, in a pathway- and cell type-specific manner.

We next ask whether the cortical subpopulations projecting to striatal D1- vs. D2-SPNs could differently control action learning. We first performed experiments in the D1-Cre mice with viral expression of ChR2 in the striatum, and found that optogenetic stimulation of D1-SPNs robustly supported intracranial self-stimulation (ICSS) (Fig. 3N) in either DMS (Fig. 3O)

or DLS (Fig. 3P). Conversely, optogenetic stimulation of D2-SPNs, either in DMS (Fig. 3O) or DLS (Fig. 3P), did not promote ICSS behavior. These data confirmed that the D1-SPN activation in both DMS and DLS drives action learning and ICSS, while D2-SPN stimulation does not strongly support ICSS behavior (Kravitz *et al.*, 2012; Vicente *et al.*, 2016).

We then test how the striatum-projecting cortical neurons in MCC or M1 would support ICSS behavior, and whether there is any difference between activation of the D1- vs. D2-SPN projecting cortical neurons. Similar to the effects of direct striatal D1-SPN stimulation (Fig. 3O, P), optogenetic stimulation of striatal D1-SPN projecting neurons was sufficient to support ICSS behavior both in MCC (Fig. 3Q, R) and in M1 (Fig. 3Q, S). Notably, optogenetic stimulation of the cortical neurons projecting to D2-SPNs also significantly drove ICSS behavior, irrespective of whether it is in MCC (Fig. 3R) or M1 (Fig. 3S). These data suggested that optogenetic activation of either D1- or D2-SPN projecting neurons in MCC or M1 could drive reinforcement learning and support ICSS behavior.

Corticostriatal circuitry is critical for action sequence learning and execution (Geddes *et al.*, 2018; Hikosaka *et al.*, 1998; Jin and Costa, 2010; 2015; Jin *et al.*, 2014; Tanji, 2001; Tecuapetla *et al.*, 2016). In particular, striatal direct and indirect pathways have been suggested to play distinct roles in controlling learned action sequences, as D1-SPNs facilitate ongoing actions while D2-SPNs inhibit actions and mediate switching (Geddes *et al.*, 2018; Jin and Costa, 2010; 2015; Jin *et al.*, 2014; Tecuapetla *et al.*, 2016). We thus ask how the D1- vs. D2-SPN projecting neurons in MCC and M1 regulate the learned action sequences. D1- or A2a-Cre mice injected with helper viruses were trained under fixed-ratio schedule, in which a fixed amount of eight (FR8) leads to reward (Geddes *et al.*, 2018; Jin and Costa, 2010; Jin *et al.*, 2014; Tecuapetla *et al.*, 2016) (Fig. 4A; see Methods). Three weeks later, the trained animals were

injected with (EnvA) SAD-ΔG Rabies-ChR2-mCherry virus in the dorsal striatum and optic fibers were bilaterally implanted in either MCC or M1 as before. Mice were continuously trained for around 4 days after 4 days of recovery from the surgeries to allow the rabies-mediated ChR2 expression before the optogenetic experiments start (Fig. 4E). High-frequency stimulation (20Hz) of the cortical neurons projecting to D1-SPNs or D2-SPNs was delivered upon the first lever press of the FR8 sequence in randomly chosen 50% trials (Geddes *et al.*, 2018; Tecuapetla *et al.*, 2016) (Fig. 4A, E, see Methods). Stimulation of MCC inputs to D1-SPNs facilitated lever pressing over the duration of the FR8 sequence (Fig. 4B, D). Conversely, stimulation of MCC inputs to D2-SPNs slightly reduced the lever press rate over the stimulation period (Fig. 4C, D). The modulation effects on lever pressing rate were significantly different between optogenetic stimulation of D1- and D2-SPN projecting MCC neurons (Fig. 4D). On the other hand, optogenetic activation of the M1 neurons that project to D1-SPNs facilitated lever pressing during sequence execution (Fig. 4F, H), similar to the effects of MCC stimulation. However, optogenetic stimulation of the M1 neurons projecting to D2-SPNs delivered an overall facilitation effect on lever pressing (Fig. 4G, H). Overall, stimulation of either D1- or D2-SPN projecting M1 neurons facilitated lever pressing in a similar degree (Fig. 4H). These results thus revealed the highly heterogeneous functions of corticostriatal subcircuits in controlling learned action sequences, depending on both the cortical region and their cell-type specific targets in striatum.

Discussion

By taking advantage of a monosynaptic rabies tracing with optogenetics system, we have discovered a significant degree of segregation between the excitatory inputs to striatal D1- vs. D2-SPNs. Notably, the results unveiled an overall asymmetric crosstalk from the excitatory inputs of D2-SPNs onto D1-SPNs, but not vice versa. Striatal D1- and D2-SPNs receive excitatory inputs from both the cortex and thalamus (Klug *et al.*, 2018; Wall *et al.*, 2013). Since the current techniques do not allow us to isolate the inputs from a specific region to D1- vs. D2-SPNs in slice recording, these results do not exclude the possibility that there might be certain cortical or thalamic regions targeting D1- and D2-SPNs equally or even with a reverse bias. However, the overall functional organization does imply that while the excitatory inputs to D1-SPNs in general drive the striatal direct pathway, the excitatory inputs to D2-SPNs control both the striatal direct and indirect pathways. Indeed, it has been recently reported that corticospinal neurons, which project to both spinal cord and DLS, form uneven synapses onto direct and indirect pathway neurons in the DLS and preferentially target at D1- other than D2-SPNs (Nelson *et al.*, 2021). Furthermore, a series of in vivo optogenetic experiments in both MCC and M1 have further supported this notion, and demonstrated that the functionally heterogeneous corticostriatal neuronal subpopulations differently control actions, in both a cortical-region- and striatal-targeting-cell-type-specific manner. These *in vivo* functional findings in corticostriatal pathways are in consistent with the observations of *in vitro* synapse connection probability. Future studies should aim to further dissect the organization and function of pathway-specific thalamostriatal subcircuits, and determine whether they share the same principles of corticostriatal projections.

The cortical neurons projecting to striatum mainly consist of layer 2/3 and layer 5 pyramidal cells (Klug *et al.*, 2018; Wall *et al.*, 2013), including both the intratelencephalic (IT)

and pyramidal tract (PT) types of neurons (Shepherd, 2013). While some anatomical preference might exist (Lei *et al.*, 2004), it has been found that both the striatal direct and indirect pathways receive functional inputs from both the IT and PT neurons (Ballion *et al.*, 2008; Kress *et al.*, 2013). Our rabies-ChR2 tracing system allows us to further separate the cortical inputs to striatal D1- vs. D2-SPNs and selectively stimulate these specific cortical subpopulations during behavior and learning. These results have further revealed the diversity of corticostriatal cell subtypes and underscored their heterogeneous functions in behavior. Although the behavioral phenotypes of optogenetic stimulation of different cortical neuronal subpopulations are largely consistent with their functional connectivity with the striatal D1- vs. D2-SPNs, it does not necessarily suggest the observed effects were mediated completely by striatum but not through their collaterals targeting other brain regions or spinal cord (Nelson *et al.*, 2021; Shepherd, 2013). In addition, it has been known that both striatal direct and indirect pathways receive inhibitory inputs from certain GABAergic interneurons in motor cortices (Melzer *et al.*, 2017). In our behavioral experiments with optogenetic stimulation in the motor cortex, there might be possible contribution from these striatum-projecting cortical inhibitory neurons. However, given the nature of sparse distribution of the GABAergic interneurons in the cortex, it is unlikely that they dominate the observed behavioral phenotype (Melzer *et al.*, 2017). Due to the limitations of current viral approaches, one might question whether our in vivo optogenetic experiments could inadvertently activate terminals from rabies-infected neurons in cortical or thalamic regions beyond the targeted area. However, a previous optogenetic study on thalamo-cortical synapses (Cruikshank *et al.*, 2010) demonstrated that sustained optogenetic stimulation (500 ms) of ChR2-expressing presynaptic terminals induces transient, rather than sustained, action potential firing on the postsynaptic neurons. Considering the much longer stimulation durations used in our

optogenetic experiments (15 s for open-field, 1 s for ICSS, and 8 s for the FR4/FR8), it is clear that the behavioral effects of optogenetic stimulation are most likely driven by the excitation of ChR2-expressing D1- or D2-SPN projecting neurons in the targeted cortical area, rather than by efferent terminals from neurons located outside this region. Nevertheless, from the striatum point of view, the distinct behavior effect does strongly suggest that the specific information the direct vs. indirect pathway received from the cortex is somehow channeled, but at the same time, effectively coordinated by the cortex.

These results have important implications on how the corticostriatal circuitry controls actions in health and disease. The traditional model of the basal ganglia suggests that the direct and indirect pathways play opponent roles in facilitating and inhibiting action, respectively (Albin *et al.*, 1989; DeLong, 1990; Kravitz *et al.*, 2010). More recent models of basal ganglia, however, propose that the direct pathway co-activates and cooperates with the indirect pathway with the former activating the selected action and the latter inhibiting the competing actions (Cui *et al.*, 2013; Hikosaka *et al.*, 2000; Jin *et al.*, 2014; Mink, 1996; Tecuapetla *et al.*, 2016). Under more complicated behavior context, it has been previously reported that the striatal D1- and D2-SPNs are co-activated during the initiation of an action sequence, but become largely segregated during the sequence performance (Geddes *et al.*, 2018; Jin *et al.*, 2014). More specifically, the various subpopulations of striatal D1- and D2-SPNs differently change their firing activity to support the start/stop of the sequence, the execution of the elemental actions, and the switch between subsequences (Geddes *et al.*, 2018). These previous findings thus suggested that the striatal direct and indirect pathways have to dynamically coordinate their activity throughout the performance of sequential actions (Geddes *et al.*, 2018; Hikosaka *et al.*, 2019; Jin and Costa, 2015; Markowitz *et al.*, 2018; Tecuapetla *et al.*, 2016).

But how are the dynamically different activities in the striatal direct and indirect pathways generated in the circuitry? Both the striatal direct and indirect pathways are driven by the excitatory inputs from the cerebral cortex and thalamus (Bolam *et al.*, 2000; C.R. Gerfen, 2016; Pan *et al.*, 2010; Wall *et al.*, 2013). However, whether or not they receive the projections from the same presynaptic neurons, and how the input information is channeled into the two pathways for proper action control remain mostly unknown. The current study has revealed the largely segregated but asymmetrically overlapping organization of the cortical projections to striatal direct vs. indirect pathway. This specific corticostriatal organization provides a structural foundation for the striatal direct and indirect pathways to implement such a dynamic coordination of activity during sequence behavior (Geddes *et al.*, 2018; Hikosaka *et al.*, 2019; Hikosaka *et al.*, 1998; Jin and Costa, 2010; 2015; Jin *et al.*, 2014; Markowitz *et al.*, 2018; Tanji, 2001; Tecuapetla *et al.*, 2016). For instance, the dedicated cortical projections to striatal direct vs. indirect pathway are well suited for controlling sequence initiation and termination, where the activation of D1- and D2-SPNs is critical (DeLong, 1990; Geddes *et al.*, 2018). On the other hand, the overlapping cortical projections to both striatal direct and indirect pathways could be crucial for action switching, which requires proper coordination of the two pathways to inhibit current action and activate the upcoming one (DeLong, 1990; Geddes *et al.*, 2018). Our findings also predict that the striatal D1- vs. D2-SPN projecting neurons in the cerebral cortex would fire differently but activate in relation with each other during behavior. Future work should aim to understand how these two cortical subpopulations behave and coordinate to control the striatal direct and indirect pathways for action learning and selection in health and disease (Dalley and Robbins, 2017; Geddes *et al.*, 2018; Hikosaka *et al.*, 2000; Jin *et al.*, 2014; Mink, 2003;

Monteiro and Feng, 2017; Redgrave *et al.*, 2010; Shepherd, 2013).

Materials and Methods

Animals

All procedures were approved by the Salk Institute Institutional Animal Care and Use Committee and followed NIH guidelines for the care and use of laboratory animals. Group housed male and female mice (2 - 6 months old) were used in this study. Animals were housed on a 12-hour dark/12-hour light cycle (dark from 6 pm to 6 am). Heterozygous Drd1-Cre (The Jackson Laboratory, stock # 030329, GENSAT: EY217) and Adora2a-Cre (The Jackson Laboratory, stock # 036158, GENSAT: KG139) mice were obtained from MMRRC and were backcrossed to C57Bl6/J mice, stock # 000664 (> 9 generations) (Cui *et al.*, 2013; Jin *et al.*, 2014; Madisen *et al.*, 2012; Tecuapetla *et al.*, 2016). BAC reporter lines D1-eGFP (MMRRC: MMRRC_000297-MU; GENSAT: X60) and D2-eGFP (MMRRC: MMRRC_00230-UNC; GENSAT: S118) (Gong *et al.*, 2007) were crossed to Drd1-Cre (D1-Cre) and Adora2a-Cre (A2a-Cre) mice to identify D1- and D2-SPNs for electrophysiological recordings.

Surgery and viral injection

For G-deleted rabies-mediated retrograde tracing and functional determination (slice recordings) (Smith *et al.*, 2016), all surgeries were performed under aseptic conditions with animals anesthetized with ketamine (100 mg/kg) / xylazine (10 mg/kg) while mounted on a stereotaxic device (Kopf Instruments; Tujunga, CA). The skull was leveled at bregma and lambda and a small hole was drilled at the coordinate (from bregma and midline) of AP + 0.5 mm, ML ± 1.8mm. A Hamilton syringe (33-gauge needle) containing 1 µl freshly mixed AAV5/EF1α-Flex-TVA-mCherry (UNC Vector Core; Chapel Hill, NC) and AAV8/CA-Flex-RG (UNC Vector Core; Chapel Hill, NC) was slowly lowered to DV - 2.2 mm from the dura to

target dorsal central striatum. The virus cocktail was injected slowly over ~10 min, and the needle was left in place for ~5 additional minutes afterwards. Then, the needle was slowly retracted over 5 minutes to reduce the virus from moving into the needle track. After injection, mice were sutured and returned to their home cage with ibuprofen (50 mg/kg/day) in their drinking water for the following four days. They were given three weeks to allow for maximal expression of helper viruses, before they were injected with 1.5 µl of (EnvA) SAD-ΔG Rabies-eGFP or 1.5 µl of (EnvA) SAD-ΔG Rabies-ChR2-mCherry (Salk Vector Core, La Jolla, CA) on an angle (18°) to avoid labeling any neurons in the initial injection tract in the same target region. Injecting locations were identical in D1-Cre and A2a-Cre animals. All the injections were done unilaterally for anatomical and slice physiology experiments, and bilaterally for behavioral experiments.

To prepare animals for optogenetic behavior experiments testing D1- or D2-SPN projecting cortical neurons, animals were anesthetized with isoflurane (4% induction, 1-2% maintenance) and locally injected with bupivacaine to numb the incision site. The animals received bilateral injections of helper virus (TVA, RG) as before in dorsal striatum. After ~21 days of pre-training and full body weight recovered (see Operant Conditioning), the skull was exposed again, and cleaned with 4% H_2O_2 and UV-light etched with Opti-Bond All-in-One (Kerr, Orange, CA). Then 1.5 µl (EnvA) SAD-ΔG Rabies-ChR2-mCherry was bilaterally injected in each hemisphere using the same coordinates as before. Then, custom made, polished optical fibers (200 µm diameter, 0.37 NA; Thor Labs, Newton, NJ) were implanted in input regions: MCC (AP +0.2 mm, ML ±0.8 mm for skull holes, fibers penetrate into brain at 17° angle off midline with traveling distance of 1.3mm, actual fiber tips target brain at AP +0.2 mm, ML ±0.4 mm, DV -1.2 mm) or M1 (AP +0.5 mm, ML ±1.2 mm, DV -0.5 mm). The fibers were

secured with a light-curing composite (Tetric EvoFlow, Ivoclar Vivadent; Mississauga, ON). Finally, a layer of black dental cement (Lang Dental, Wheeling, IL) was added on the top of the previous cement to support and block laser light diffusion during stimulation. Animals were given ibuprofen in their drinking water for pain management during post-surgery recovery (4 days).

For striatal opto-ICSS and open field experiments, D1- or A2a-Cre mice were injected bilaterally with AAV5-EF1α-DIO-ChR2(H134R)-mCherry (Salk Vector Core, La Jolla, CA) in DMS (AP 0.5 mm, ML ±1.5 mm, DV -2.2 mm) or DLS (AP 0.5 mm, ML ±2.5 mm, DV -2.2 mm), and fiber optics were implanted ~0.2 mm above the injection site. In control experiments for testing striatal activation by light penetration from cortical optic fibers (Fig S3), D1- or A2a-Cre mice were injected with AAV5-EF1α-DIO-ChR2(H134R)-mCherry bilaterally in DMS, and fiber optics were bilaterally implanted into M1 of the same coordinates as previously described.

Ex vivo brain slice electrophysiology

4-8 days were allowed for expression and optimal cell health post unilateral (EnvA) SAD-ΔG Rabies-ChR2-mCherry injection before electrophysiology recordings on acute slice were carried out (Klug *et al.*, 2017; Smith *et al.*, 2016). Mice were anesthetized with ketamine/xylazine and transcardially perfused with ~20 mL ice-cold, bubbling (95% O_2/5% CO_2) NMDG cutting solution [consisting of (in mM): NMDG 105, HCl 105, KCl 2.5, NaH_2PO_4 1.2, $NaHCO_3$ 26, Glucose 25, Sodium L-Ascorbate 5, Sodium Pyruvate 3, Thiourea 2, $MgSO_4$ 10, $CaCl_2$ 0.5, 300 mOsm, pH = 7.4]. The extracted brain was blocked coronally with a brain matrix (Zivic Instruments; Pittsburg, PA) and acute coronal slices (300 µm) were cut on a vibratome (VT1000S, Leica Microsystems; Buffalo Grove, IL) through the striatum in ice-cold,

bubbling NMDG based cutting solution. Slices recovered for 15 minutes at 32 °C in bubbling NMDG cutting solution, then transferred to a holding chamber containing normal aCSF [consisting of (in mM): NaCl 125, KCl 2.5, NaH_2PO_4 1.25, $NaHCO_3$ 25, D-Glucose 12.5, $MgCl_2$ 1, $CaCl_2$ 2, pH = 7.4, 295 mOsm] bubbling (95% O_2/5% CO_2) at 28 °C. At least one hour after recovery, the slices were placed in the recording chamber, in which normal aCSF (33~34 °C, bubbling with 95% O_2/ 5% CO_2) was perfused over the slices at ~2 mL/min throughout recordings. Dorsal striatal SPNs were visualized under IR-DIC optics (Zeiss Axioskop2; Oberkocken, Germany) at 40x and D1- or D2-SPNs were confirmed by eGFP expression with brief observation in the epifluorescent channel. D1-SPNs (eGFP-positive in D1-eGFP mice, or eGFP-negative in D2-eGFP mice) or D2-SPNs (eGFP-positive in D2-eGFP mice, or eGFP-negative in D1-eGFP mice) that were ChR2-mCherry-negative, but in the injection site and surrounded by cells expressing ChR2-mCherry were targeted for recording. Only animals with high efficiency labeling throughout the cortex were used for recordings to determine collateralization.

Voltage clamp recordings were performed using 3-4 MΩ patch pipettes (WPI; Sarasota, FL), which were pulled from borosilicate glass on a P-97 pipette puller (Sutter Instruments; Novato, CA) and filled with a Cs^+ methanesulfonate based internal solution [consisting of (in mM): $CsMeSO_3$ 120, NaCl 5, TEA-Cl 10, HEPES 10, QX-314 5 EGTA 1.1, Mg-ATP 4, Na-GTP 0.3, pH = 7.2-7.3, 305 mOsm]. All cells were voltage clamped at -70 mV during recording. Five minutes post break-in, paired light pulses (473nm, 5-25 mW/mm^2, 2.5 ms, 50 ms ISI) were delivered through a glass fiber optic (200 µm in diameter, Thor Labs; Newton, NJ), positioned close to the recorded cell (50-150 µm), at 0.05 Hz using a 473 nm blue DPSS laser system (Laserglow Technologies, Toronto, ON). Light evoked currents were collected after at least 8-10

minutes of bath application 50 - 100 µM picrotoxin (MilliporeSigma, St. Louis, MO) to block any ChR2-mediated fast $GABA_AR$ transmission. Twenty sweeps were collected to determine latency and CV. At the end of experiments, both 10 µM NBQX (AMPAR antagonist) and 50 µM DL-APV (NMDAR antagonist) (MilliporeSigma, St. Louis, MO) were applied to block AMPAR and NMDAR-mediated transmission, respectively to confirm the EPSCs. Series resistance was initially compensated and monitored continuously throughout the experiment, and the data were rejected if the series resistance changed by more than 20% over the duration of the recording. A cell is considered connected if it has a detectable, reliable current (20 sweeps, 0.05 Hz) with onset latency less than 10 ms post laser-on (Klug *et al.*, 2017; Smith *et al.*, 2016). Voltage clamp recordings were digitized at 10 kHz and filtered at 2 kHz.

For current clamp recordings of rabies-positive pyramidal neurons in the cortex, a potassium methanesulfonate based internal solution [(in mM): $KMeSO_4$ 135, KCl 5, $CaCl_2$ 0.5, HEPES 5, EGTA 5, Mg-ATP 2, Na-GTP 0.3, (pH = 7.3, 305 mOsm)] was used. 750 ms current injections (-250 to 200 pA) were given to test the membrane potential response of rabies-ChR2 positive pyramidal neurons, in primary motor cortex layer 5, and followed by 20 Hz or 5 Hz optogenetic stimulation to test the response of these neurons to light. Current clamp recordings were filtered and digitized at 10 kHz. All recordings were performed using a Multiclamp 700A amplifier (Molecular Devices; Sunnyvale, CA), digitized with Digidata 1440 (Molecular Devices; Sunnyvale, CA) and collected with pClamp 9 software (Molecular Devices; Sunnyvale, CA). Data were analyzed with Clampfit 9.

<u>Open field</u>

After helper viruses' injections in the striatum, animals were put back on food and allowed to recover and viral expression. They were then injected with (EnvA) SADΔG-ChR2-mCherry virus in the striatum and implanted with fiber optics in the MCC or M1 as described above (see Surgery and Viral Injection). Then animals were allowed to recover over 3 days. On the fourth day post injection and implantation, animals went through open field test. They were connected to fiber-optic leads (Doric) that connected to a laser through a commutator for free movement. An additional light shield was attached at fiber optic connection to the mouse to mask the laser light output. Following habituation to the fiber optic connections in a home cage the mice were placed in the middle of a 41cm x 41cm square, white and evenly illuminated open field chamber. Custom MEDPC code delivered 20 Hz or 5 Hz stimulation (473 nm blue laser, 5 mW power at connection to mouse, 10 ms pulse width) for 15 seconds after every 3 minutes and 45 seconds, and each animal received 3-4 replicates. Mice with AAV5-EF1α-DIO-ChR2(H134R)-mCherry injected bilaterally in DMS or DLS went through similar open field test after 4 days of recovery from surgery, with optic stimulation in DMS, DLS or M1. Video was collected for each run and analyzed in Ethovision 8.5. To analyze the open field data, the behavior was binned in 10-s bins and distance traveled during laser on period was normalized to the averaged distances during preceding 45 s just prior to stimulation onset.

<u>Optogenetic intracranial self-stimulation (opto-ICSS)</u>

In opto-ICSS experiments, two different subsets of animals were used: to stimulate D1- and D2-SPNs in DMS and DLS, or to stimulate D1- or D2-SPN-projecting cortical neurons in MCC and M1, respectively. Mice that had never experienced the operant chamber were injected with virus and implanted with fiber optics using the procedure described above. From the fourth

day following surgery, the mice received ICSS training for 7 consecutive days. They were attached to fiber-optic patch cords and placed in an operant chamber. Each session began with the illumination of a house light and the extension of two levers: one active (left) and one inactive (right). Every time the mouse pressed the active lever, a 20 Hz stimulation was triggered (473 nm blue laser, 5 mW power at connection to mouse, 10 ms pulse width, 1 s duration) targeting the cell bodies in MCC or M1 that project to D1- or D2-SPNs. Each session concludes after 90 minutes with the retraction of the levers and the house light turning off. Continuous pressing of the lever during stimulation will not lengthen the stimulation period. Pressing of the inactive lever had no consequence and was used as a control of general activity measure of non-contingent lever pressing. All protocols were custom written in MEDPC (Med Associates).

Sequence training and optogenetic stimulation

Prior to the injection of the rabies virus, animals were pre-trained for three weeks in fixed ratio 8 (FR8) or fixed ratio 4 (FR4) task (Jin *et al.*, 2010; Jin *et al.*, 2014). Briefly, animals were food-restricted (30 hrs) to start training and weighed daily to monitor their bodyweight. They were fed approximately 2-2.5 g regular chow/mouse/day after each behavioral training session concluded to maintain around 85% of their initial weight. Animals were trained in operant chambers (21.6 cm (L) x 17.8 cm (W) x 12.7 cm (H)) housed in a sound attenuating box (Med-Associates, St. Albans, VT) with two retractable levers to the left and right of a central food magazine and a house light (3 W, 24 V) opposite to the levers and magazine. Sucrose solution (15 µl, 10%) was delivered by a syringe pump into a metal bowl as a reinforcer. Magazine entries were recorded using an infrared beam break detector. Behavioral chambers were

controlled by MED-PC IV software (MED Associates, VT) that recorded all timestamps of lever presses and magazine entries with a resolution of 10 ms.

Operant training began with continuous reinforcement (CRF) also known as fixed ratio 1 (FR1) in which animals received a reinforcer following each lever press. The animals were trained on CRF for both levers (separate flanking sessions) over three days and the order of lever presentation was counterbalanced. Each session began with the illumination of the house light and the extension of one lever. The session ended with the offset of the house light and retraction of the lever after 90 minutes of training or after a reinforcer cap was reached. On day 1, 2, 3, the mice could earn up to 10, 15, or 30 sucrose reinforcers, respectively. After the animals acquired CRF over 3 days, they were transitioned to FR4 and FR8 schedules on independent levers and the order counterbalanced. The session began with the illumination of the house light and the extension of either the left or right lever. Following four consecutive lever presses (FR4), mice received a reinforcer in a central magazine port. There was no time requirement for completion of the action sequence. The session concluded with the retraction of the lever and the offset of the house light after the mouse received either 80 reinforcers or 90 minutes expired. Another session was given just following the conclusion of the FR4 session, where eight consecutive lever presses (FR8) on the opposite lever resulted in the delivery of a sucrose reinforcer. The order of training FR4 or FR8 was randomly shuffled over 21 days pre-training. Left and right levers were randomly assigned FR4 or FR8 schedules and that set up was maintained for each animal over pre-training.

On the fourth day after rabies injection and fiber optic implant, and after open field test, the mice were food deprived for 24 hours to start optogenetic test in sequence tasks. On the fifth day, the animals were tethered to two fiber-optic patch cables attached to a commutator (Doric,

Canada) to allow for free rotation and placed back in the original pre-training operant box. They were given three days of re-training in a session of FR4 on one lever and subsequent session of FR8 on the opposite lever with fiber attached (90-minute session, 80 reinforcers max). The order of the sessions was randomly shuffled. If the animals successfully completed 80 reinforcers, they were transitioned to optogenetic stimulation test session. On day 8 post rabies injection, optogenetic stimulations (20 Hz, 473 nm blue laser, 5 mW power at connection to mouse, 10 ms pulse width) were randomly delivered for 8 seconds (a time period covering roughly the entire lever press sequence) on the first press (defined by the first lever press after either head entry or 2-second break after the reward delivery) with a 50% likelihood of control non-stimulated trials randomly interleaved (Geddes *et al.*, 2018). Stimulus conditions were repeated on multiple days if needed to collect enough trials for statistics. On day 12 post rabies injection, the animals were perfused for histology analysis.

All sequence data were analyzed in MATLAB using custom scripts. To construct the peri-event time histograms (PETH), all lever presses before the reward (control or stimulation trials) were aligned to the first press of the FR4 or FR8 sequence, averaged in 100 ms bins, and filtered with a Gaussian low-pass filter (window size = 5, standard deviation = 5). All the PETHs were plotted with the first press omitted for illustration and comparison clarity. The effects of optogenetic modulation on press rate were qualitatively similar for FR4 and FR8 sequences and thus combined for statistics.

<u>Histology and microscopy</u>

Approximately twelve days following rabies injection or after behavior tests, mice were anesthetized with an overdose of ketamine/xylazine and transcardially perfused with 0.01 M PBS

(30-40 mL) followed by 4% paraformaldehyde (PFA)/0.1 M PB, pH 7.4 (30-40 mL), with a peristaltic perfusion pump (Cole Parmer, Vernon Hills, IL) (Klug *et al.*, 2017; Smith *et al.*, 2016). The brain was carefully extracted and post-fixed in 4% PFA/0.1 M PB overnight (16-24 hrs), then transferred to 30% sucrose/0.1 M PB for 1-2 days until the brain equilibrated and sunk. On the day of cutting, it was coronally blocked with a brain matrix (Zivic Instruments; Pittsburg, PA) and mounted on a freezing microtome. Coronal slices were collected from the most rostral to the most caudal sites at 50 µm resolution in 96 well plates containing cryoprotectant (0.1 M phosphate buffer, ethylene glycol, glycerol) to maintain AP position. Brain slices surrounding the injection site and fiber implant site were mounted on super frost plus slides (Thermo Fisher Scientific, Waltham, MA), counterstained for DAPI and cover slipped with Aqua-Poly/Mount mounting media (Polysciences, Inc; Warrington, PA). Slides were scanned on an automated slide scanner (Olympus VS120) at 10x in the blue and red channels. Images were batch converted to composite TIFFs and saved for image analysis.

Statistics

Statistics were conducted in Graph Pad Prism 6.01 (La Jolla, CA). Fisher's exact-test was used in comparing the likelihood of connections in slice recordings. Student unpaired two-tailed t-test was used in open field test and sequence operant task to analyze optogenetic stimulation effects. Non-parametric Mann Whitney U Test was conducted when distributions significantly deviated from normal distributions. The reinforcing effect of each group in the ICSS task was assessed using a permutation test (10,000 permutations per group). A one-sample two-tailed t-test or Wilcoxon signed-rank test was used to assess the effectiveness of optogenetic activation in each individual group during the sequence operant task.

Supplementary Information

Supplemental Information includes 3 Supplemental Figures and Supplemental Experimental Procedures.

Acknowledgements

The authors would like to thank Tom Jessell, Chris Kintner and members of the Jin lab for discussion and comments on the manuscript. This work was supported by grants from the NIH (R01NS083815), the Dystonia Medical Research Foundation and the McKnight Memory and Cognitive Disorders Award to X.J.

Author Contributions

X.J. conceived the project. J.R.K. and X.J. designed the experiments. J.R.K., X.Y. performed the rabies tracing, slice electrophysiology, behavioral experiments and analyzed the data. H.A.H. assisted the viral injections. M.D.E. conducted the cell counting. F.O. and E.M.C. provided the (EnvA)-ΔG-Rabies-ChR2-mCherry virus. J.R.K and X.Y. constructed the figures. J.R.K., X.Y. and X.J. wrote the manuscript.

Conflict of Interest

None of the authors declare any conflict of interest, financial or otherwise.

References:

Albin, R.L., Young, A.B., and Penney, J.B. (1989). The functional anatomy of basal ganglia disorders. Trends Neurosci *12*, 366-375.

Aoki, S., Smith, J.B., Li, H., Yan, X., Igarashi, M., Coulon, P., Wickens, J.R., Ruigrok, T.J., and Jin, X. (2019). An open cortico-basal ganglia loop allows limbic control over motor output via the nigrothalamic pathway. Elife *8*, e49995.

Ballion, B., Mallet, N., Bezard, E., Lanciego, J.L., and Gonon, F. (2008). Intratelencephalic corticostriatal neurons equally excite striatonigral and striatopallidal neurons and their discharge activity is selectively reduced in experimental parkinsonism. Eur J Neurosci *27*, 2313-2321.

Bolam, J.P., Hanley, J.J., Booth, P.A., and Bevan, M.D. (2000). Synaptic organisation of the basal ganglia. J Anat *196 (Pt 4)*, 527-542.

C.R. Gerfen, J.P.B. (2016). The Neuroanatomical Organization of the Basal Ganglia. In Handbook of Basal Ganglia Structure and Function, K.Y.T. Heinz Steiner, ed. (Elsevier), pp. 3-32.

Cruikshank, S.J., Urabe, H., Nurmikko, A.V., and Connors, B.W. (2010). Pathway-Specific Feedforward Circuits between Thalamus and Neocortex Revealed by Selective Optical Stimulation of Axons. Neuron *65*, 230-245.

Cui, G., Jun, S.B., Jin, X., Pham, M.D., Vogel, S.S., Lovinger, D.M., and Costa, R.M. (2013). Concurrent activation of striatal direct and indirect pathways during action initiation. Nature *494*, 238-242.

Dalley, J.W., and Robbins, T.W. (2017). Fractionating impulsivity: neuropsychiatric implications. Nat Rev Neurosci *18*, 158-171.

DeLong, M.R. (1990). Primate models of movement disorders of basal ganglia origin. Trends Neurosci *13*, 281-285.

Geddes, C.E., Li, H., and Jin, X. (2018). Optogenetic Editing Reveals the Hierarchical Organization of Learned Action Sequences. Cell *174*, 32-43 e15.

Gerfen, C.R., Engber, T.M., Mahan, L.C., Susel, Z., Chase, T.N., Monsma, F.J., Jr., and Sibley, D.R. (1990). D1 and D2 dopamine receptor-regulated gene expression of striatonigral and striatopallidal neurons. Science *250*, 1429-1432.

Gong, S., Doughty, M., Harbaugh, C.R., Cummins, A., Hatten, M.E., Heintz, N., and Gerfen, C.R. (2007). Targeting Cre recombinase to specific neuron populations with bacterial artificial chromosome constructs. J Neurosci *27*, 9817-9823.

Graybiel, A.M. (1998). The basal ganglia and chunking of action repertoires. Neurobiol Learn Mem *70*, 119-136.

Haber, S.N. (2016). Corticostriatal circuitry. Dialogues Clin Neurosci *18*, 7-21.

Hikosaka, O., Kim, H.F., Amita, H., Yasuda, M., Isoda, M., Tachibana, Y., and Yoshida, A. (2019). Direct and indirect pathways for choosing objects and actions. Eur J Neurosci *49*, 637-645.

Hikosaka, O., Miyashita, K., Miyachi, S., Sakai, K., and Lu, X. (1998). Differential roles of the frontal cortex, basal ganglia, and cerebellum in visuomotor sequence learning. Neurobiol Learn Mem *70*, 137-149.

Hikosaka, O., Takikawa, Y., and Kawagoe, R. (2000). Role of the basal ganglia in the control of purposive saccadic eye movements. Physiol Rev *80*, 953-978.

Jin, X., and Costa, R.M. (2010). Start/stop signals emerge in nigrostriatal circuits during sequence learning. Nature *466*, 457-462.

Jin, X., and Costa, R.M. (2015). Shaping action sequences in basal ganglia circuits. Curr Opin Neurobiol *33*, 188-196.

Jin, X., Tecuapetla, F., and Costa, R.M. (2014). Basal ganglia subcircuits distinctively encode the parsing and concatenation of action sequences. Nat Neurosci *17*, 423-430.

Klug, J.R., Engelhardt, M.D., Cadman, C.N., Li, H., Smith, J.B., Ayala, S., Williams, E.W., Hoffman, H., and Jin, X. (2018). Differential inputs to striatal cholinergic and parvalbumin interneurons imply functional distinctions. Elife *7*, e35657.

Kravitz, A.V., Freeze, B.S., Parker, P.R., Kay, K., Thwin, M.T., Deisseroth, K., and Kreitzer, A.C. (2010). Regulation of parkinsonian motor behaviours by optogenetic control of basal ganglia circuitry. Nature *466*, 622-626.

Kravitz, A.V., Tye, L.D., and Kreitzer, A.C. (2012). Distinct roles for direct and indirect pathway striatal neurons in reinforcement. Nat Neurosci *15*, 816-818.

Kress, G.J., Yamawaki, N., Wokosin, D.L., Wickersham, I.R., Shepherd, G.M., and Surmeier, D.J. (2013). Convergent cortical innervation of striatal projection neurons. Nat Neurosci *16*, 665-667.

Kupferschmidt, D.A., Juczewski, K., Cui, G., Johnson, K.A., and Lovinger, D.M. (2017). Parallel, but Dissociable, Processing in Discrete Corticostriatal Inputs Encodes Skill Learning. Neuron *96*, 476-489 e475.

Lei, W., Jiao, Y., Del Mar, N., and Reiner, A. (2004). Evidence for differential cortical input to direct pathway versus indirect pathway striatal projection neurons in rats. J Neurosci *24*, 8289-8299.

Madisen, L., Mao, T., Koch, H., Zhuo, J.M., Berenyi, A., Fujisawa, S., Hsu, Y.W., Garcia, A.J., 3rd, Gu, X., Zanella, S., et al. (2012). A toolbox of Cre-dependent optogenetic transgenic mice for light-induced activation and silencing. Nat Neurosci *15*, 793-802.

Markowitz, J.E., Gillis, W.F., Beron, C.C., Neufeld, S.Q., Robertson, K., Bhagat, N.D., Peterson, R.E., Peterson, E., Hyun, M., Linderman, S.W., et al. (2018). The Striatum Organizes 3D Behavior via Moment-to-Moment Action Selection. Cell *174*, 44-58 e17.

Melzer, S., Gil, M., Koser, D.E., Michael, M., Huang, K.W., and Monyer, H. (2017). Distinct Corticostriatal GABAergic Neurons Modulate Striatal Output Neurons and Motor Activity. Cell Rep *19*, 1045-1055.

Mink, J.W. (1996). The basal ganglia: focused selection and inhibition of competing motor programs. Prog Neurobiol *50*, 381-425.

Mink, J.W. (2003). The Basal Ganglia and involuntary movements: impaired inhibition of competing motor patterns. Arch Neurol *60*, 1365-1368.

Monteiro, P., and Feng, G. (2017). SHANK proteins: roles at the synapse and in autism spectrum disorder. Nat Rev Neurosci *18*, 147-157.

Nelson, A., Abdelmesih, B., and Costa, R.M. (2021). Corticospinal populations broadcast complex motor signals to coordinated spinal and striatal circuits. Nat Neurosci *24*, 1721-1732.

Osakada, F., Mori, T., Cetin, A.H., Marshel, J.H., Virgen, B., and Callaway, E.M. (2011). New rabies virus variants for monitoring and manipulating activity and gene expression in defined neural circuits. Neuron *71*, 617-631.

Pan, W.X., Mao, T., and Dudman, J.T. (2010). Inputs to the dorsal striatum of the mouse reflect the parallel circuit architecture of the forebrain. Front Neuroanat *4*, 147.

Redgrave, P., Rodriguez, M., Smith, Y., Rodriguez-Oroz, M.C., Lehericy, S., Bergman, H., Agid, Y., DeLong, M.R., and Obeso, J.A. (2010). Goal-directed and habitual control in the basal ganglia: implications for Parkinson's disease. Nat Rev Neurosci *11*, 760-772.

Shepherd, G.M. (2013). Corticostriatal connectivity and its role in disease. Nat Rev Neurosci *14*, 278-291.

Smith, J.B., Klug, J.R., Ross, D.L., Howard, C.D., Hollon, N.G., Ko, V.I., Hoffman, H., Callaway, E.M., Gerfen, C.R., and Jin, X. (2016). Genetic-Based Dissection Unveils the Inputs and Outputs of Striatal Patch and Matrix Compartments. Neuron *91*, 1069-1084.

Stephenson-Jones, M., Samuelsson, E., Ericsson, J., Robertson, B., and Grillner, S. (2011). Evolutionary conservation of the basal ganglia as a common vertebrate mechanism for action selection. Curr Biol *21*, 1081-1091.

Tanji, J. (2001). Sequential organization of multiple movements: involvement of cortical motor areas. Annu Rev Neurosci *24*, 631-651.

Tecuapetla, F., Jin, X., Lima, S.Q., and Costa, R.M. (2016). Complementary Contributions of Striatal Projection Pathways to Action Initiation and Execution. Cell *166*, 703-715.

van Heukelum, S., Mars, R.B., Guthrie, M., Buitelaar, J.K., Beckmann, C.F., Tiesinga, P.H.E., Vogt, B.A., Glennon, J.C., and Havenith, M.N. (2020). Where is Cingulate Cortex? A Cross-Species View. Trends Neurosci *43*, 285-299.

Vicente, A.M., Galvao-Ferreira, P., Tecuapetla, F., and Costa, R.M. (2016). Direct and indirect dorsolateral striatum pathways reinforce different action strategies. Curr Biol *26*, R267-269.

Vogt, B.A., and Paxinos, G. (2014). Cytoarchitecture of mouse and rat cingulate cortex with human homologies. Brain Struct Funct *219*, 185-192.

Wall, N.R., De La Parra, M., Callaway, E.M., and Kreitzer, A.C. (2013). Differential innervation of direct- and indirect-pathway striatal projection neurons. Neuron *79*, 347-360.

Yin, H.H., and Knowlton, B.J. (2006). The role of the basal ganglia in habit formation. Nat Rev Neurosci *7*, 464-476.

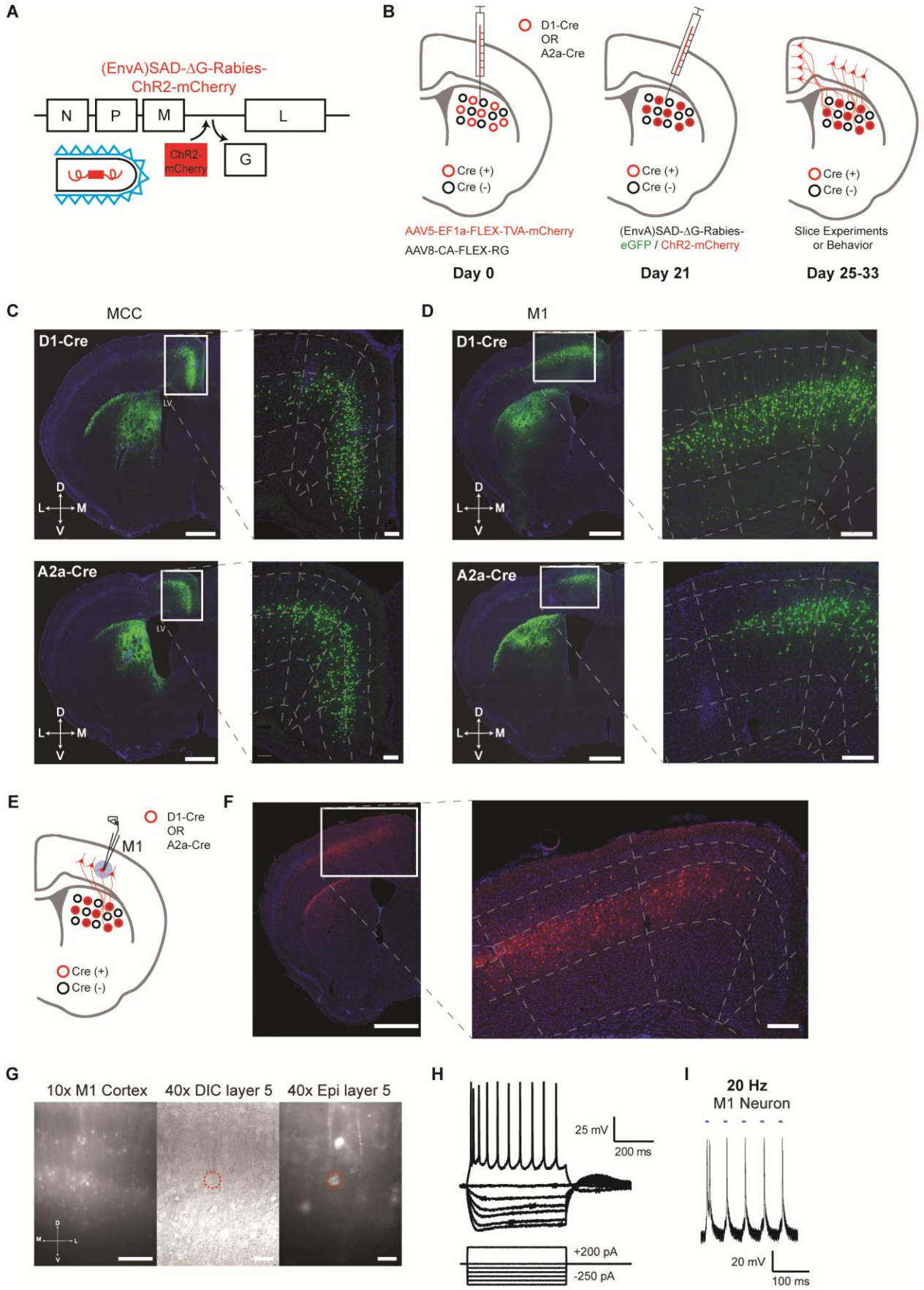
A
(EnvA)SAD-ΔG-Rabies-
ChR2-mCherry
N
P
M
L
ChR2-
mCherry
G
B
D1-Cre
OR
A2a-Cre
Cre (+)
Cre (-)
AAV5-EF1a-FLEX-TVA-mCherry
AAV8-CA-FLEX-RG
Day 0
(EnvA)SAD-ΔG-Rabies-
eGFP / ChR2-mCherry
Day 21
Slice Experiments
or Behavior
Day 25-33
C
MCC
D1-Cre
A2a-Cre
LV
D
M
L
V
D
M1
E
M1
F
G
10x M1 Cortex
40x DIC layer 5
40x Epi layer 5
H
25 mV
200 ms
+200 pA
-250 pA
I
20 Hz
M1 Neuron
20 mV
100 ms

Figure 1. Selective labeling and functional expression of ChR2 in specific cortical neurons projecting to striatal D1- vs. D2-SPNs. (A) Schematic of SAD-ΔG-Rabies-ChR2-mCherry construct with the glycoprotein deleted and replaced with ChR2-mCherry. **(B)** Timeline of viral injections of Cre-dependent helper viruses and the modified rabies virus for slice and behavioral experiments. **(C)** Example of coronal brain section with rabies-eGFP injection in the dorsal medial striatum of D1-Cre (top) or A2a-Cre (bottom) mouse shows enriched eGFP expression in the MCC. Scale bar, 1 mm. Inset (right): Higher magnification of retrogradely-labeled striatal D1- or D2-SPN projecting neurons in the MCC expressing eGFP. Dotted lines demarcate cortical lamina. Scale bar, 200 µm. **(D)** Similar experiments of labeling striatal D1- vs. D2-SPN projecting neurons in M1 with rabies-eGFP. **(E)** Cartoon brain schematic of ChR2-mCherry expressing M1 neurons projecting to SPNs (red) during whole-cell patch clamp recordings. **(F)** Example of coronal brain section with rabies-ChR2-mCherry injection in the dorsal lateral striatum of A2a-Cre mouse. Scale bar, 1 mm. Inset (right): Higher magnification of retrogradely-labeled striatal D2-SPN projecting neurons in the M1 showed clear membrane expression of ChR2-mCherry. Scale bar, 200 µm. **(G)** (left) 10x epifluorescent (red channel) of ChR2-mCherry positive neurons in M1. Scale bar, 250 µm. (middle) 40x image of a patched layer 5 pyramidal neuron under DIC optics. Scale bar, 50 µm. (right) Epifluorescent image (red channel) showing patched layer 5 pyramidal neuron somas expressing ChR2-mCherry signal. Red dotted line denotes patched neuron. Scale bar, 50 µm. **(H)** Current-voltage traces of a ChR2-mCherry positive layer 5 M1 neuron under current clamp responding to hyperpolarizing and depolarizing current injection steps. Scale bars, 200 ms, 25 mV. **(I)** Optogenetic stimulation (20 Hz) elicits robust action potentials with high fidelity in a ChR2-mCherry positive D1-SPN projecting M1 neuron in layer 5. Scale bars, 100 ms, 20 mV.

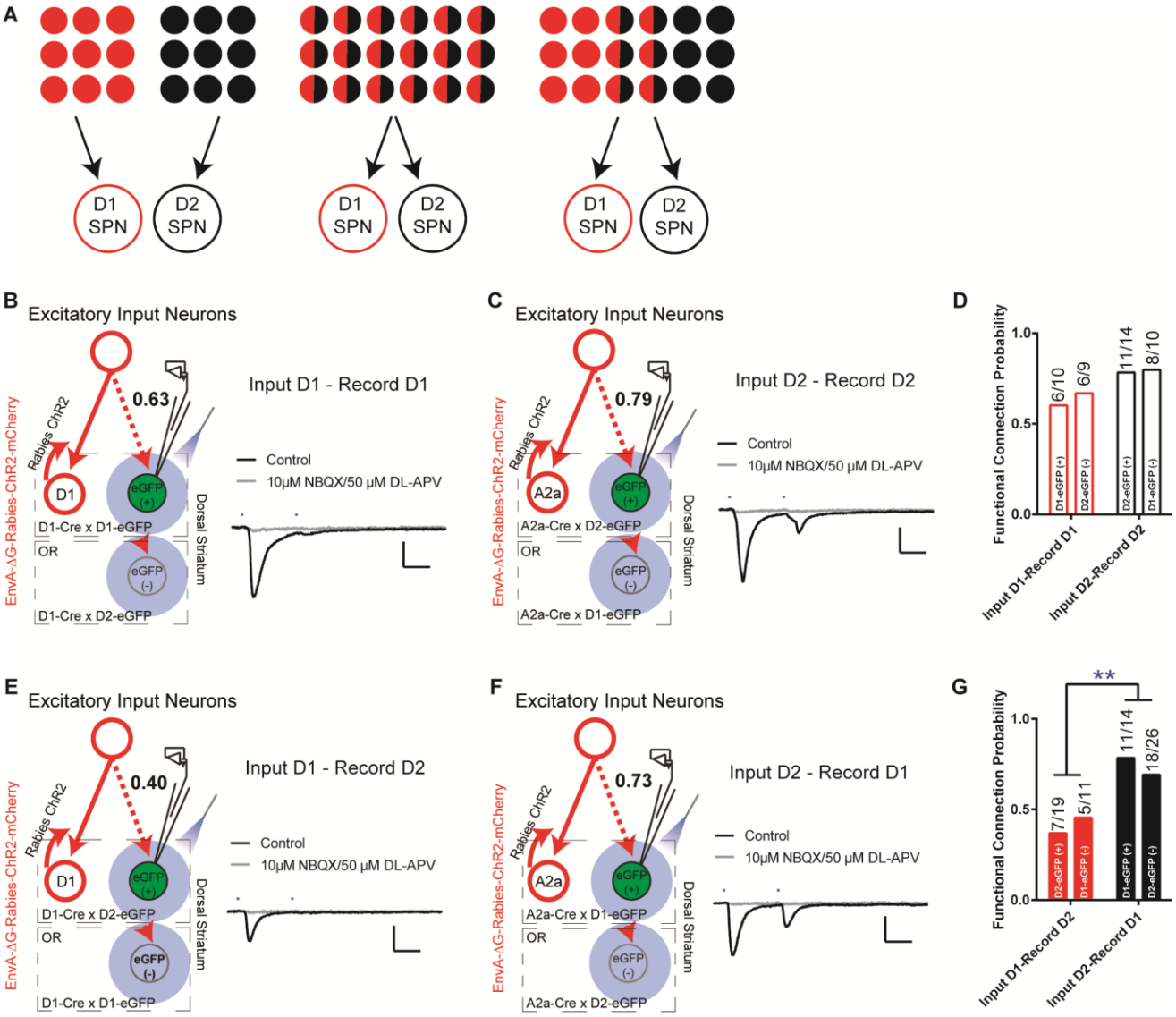

Figure 2. The excitatory inputs to striatal D1- vs. D2-SPNs are partially segregated with asymmetrical overlapping. (A) Schematic for the possible organization of the excitatory inputs to striatal D1- vs. D2-SPNs from completely segregated (left), totally overlapping (middle), to partially mixed (right). The red and black filled circles indicate the individual neurons projecting to D1- vs. D2-SPNs, respectively. The half red and half black circles imply the neurons projecting to both. **(B)** (left) Schematic of rabies-ChR2 labeling of the inputs to D1-SPNs and whole-cell recordings of rabies-negative striatal D1-SPNs with local optogenetic stimulation. (right) Example of the average EPSC trace showing short latency response to paired pulses (50 ms ISI) stimulation (black), that is blocked by AMPAR and NMDAR antagonists (gray). All recordings were conducted in the presence of picrotoxin (PTX) to isolate excitatory transmission. Scale bar, 25 ms, 100 pA. Same conditions applied to all following recordings. **(C)** Whole-cell recording of rabies-negative striatal D2-SPNs with local optogenetic stimulation with rabies-ChR2 labeling of the inputs to D2-SPNs. **(D)** The likelihood of the inputs to D1-SPNs form a functional connection with nearby non-starter D1-SPNs, and the likelihood of the D2-SPN situation. Numbers above the bars denote number of cells that show functional connectivity within total recorded. Fisher's exact test, $P = 0.3137$. Number of animals in each group: D1-projecting to D1 EGFP(+), $N = 7$; D1-projecting to D2 EGFP(-), $N = 8$; D2-projecting to D2 EGFP(+), $N = 10$; D2-projecting to D1 EGFP(-), $N = 8$. **(E-F)** Whole-cell recording of rabies-negative striatal D2-SPNs with local optogenetic stimulation with rabies-ChR2 labeling of the inputs to D1-SPNs (E), and recording of rabies-negative D1-SPNs with stimulation of inputs to D2-SPNs (F). **(G)** The likelihood of the inputs to D1-SPNs form a functional connection with nearby non-starter D2-SPNs, and the likelihood of the inputs to

D2-SPNs form a functional connection with nearby non-starter D1-SPNs. Fisher's exact test, $P = 0.0079$. **, $P < 0.01$. Number of animals in each group: D1-projecting to D2 EGFP(+), $N = 8$; D1-projecting to D1 EGFP(-), $N = 7$; D2-projecting to D1 EGFP(+), $N = 8$; D2-projecting to D2 EGFP(-), $N = 10$.

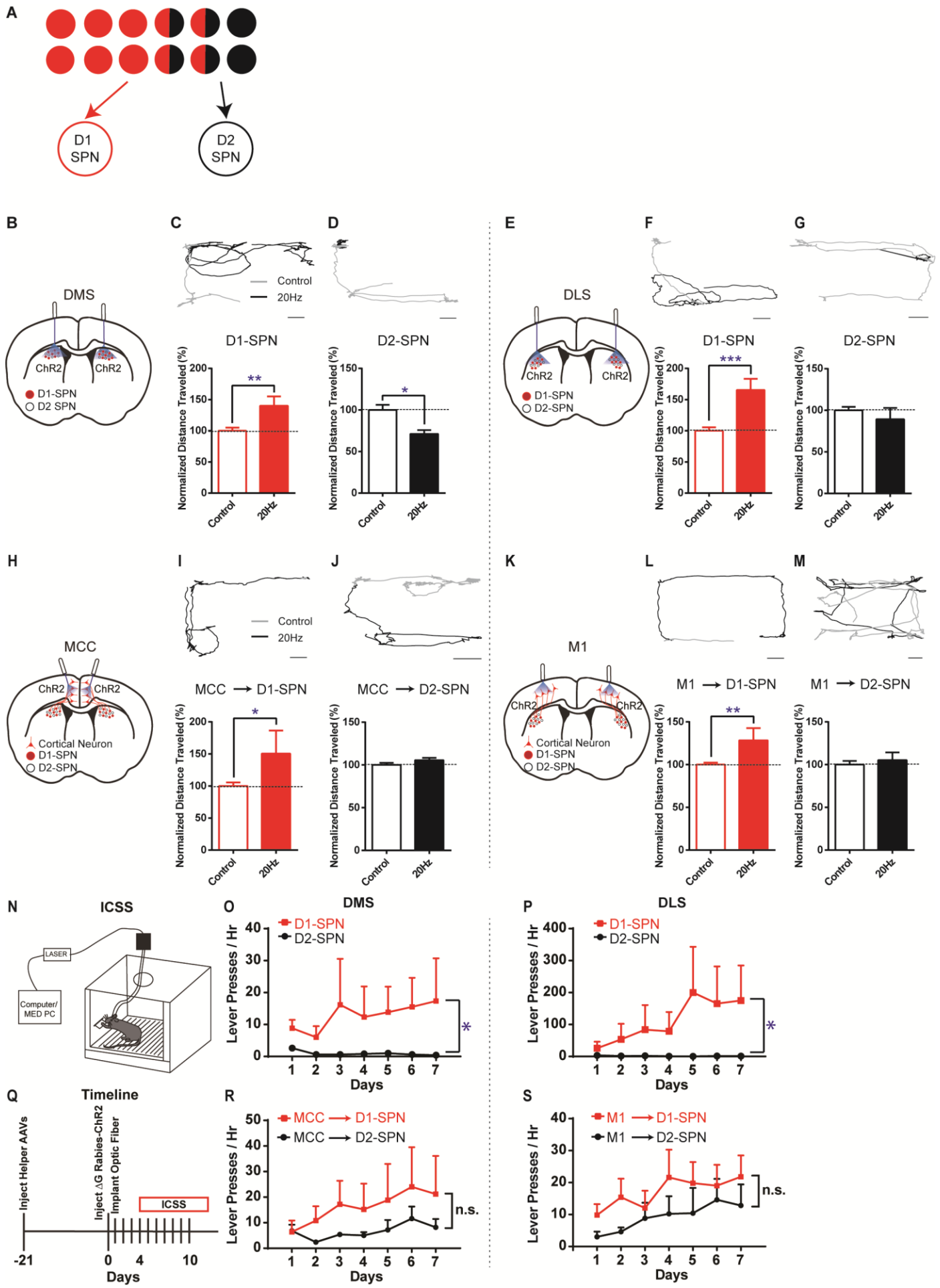
A
D1 SPN
D2 SPN
B
DMS
ChR2
ChR2
D1-SPN
D2 SPN
C
Control
20Hz
D1-SPN
Normalized Distance Traveled (%)
**
Control
20Hz
D
D2-SPN
*
E
DLS
D1-SPN
D2-SPN
F
D1-SPN
***
G
D2-SPN
H
MCC
Cortical Neuron
D1-SPN
D2-SPN
I
MCC → D1-SPN
J
MCC → D2-SPN
K
M1
L
M1 → D1-SPN
M
M1 → D2-SPN
N
ICSS
LASER
Computer/ MED PC
O
DMS
Lever Presses / Hr
Days
P
DLS
Q
Timeline
Inject Helper AAVs
Inject ΔG Rabies-ChR2
Implant Optic Fiber
ICSS
-21
0
4
10
R
MCC → D1-SPN
MCC → D2-SPN
n.s.
S
M1 → D1-SPN
M1 → D2-SPN

Figure 3. Different effects of optogenetic stimulation of D1- vs. D2-SPN projecting cortical neurons on locomotion and reinforcement learning. (A) Schematic of largely segregated yet partially overlapping excitatory inputs to striatal D1- vs. D2-SPNs. **(B)** Schematic of dorsal medial striatum (DMS) injection of Cre-dependent AAV-ChR2 and optogenetic simulation in D1- or A2a-Cre mice. **(C)** (top) Example of locomotion path under control (black) and following 20Hz optogenetic stimulation (gray) of DMS D1-SPNs in open field. Scale bar, 5cm, same for below. (bottom) Stimulation of D1-SPNs in DMS facilitates locomotion (n = 5, unpaired two-tailed t-test, t = 3.386, P = 0.0046). **, P < 0.01. **(D)** 20Hz stimulation of D2-SPNs in DMS suppresses locomotion (n = 5, unpaired two-tailed t-test, t = 2.559, P = 0.0227). *, P < 0.05. **(E)** Schematic for dorsal lateral striatum (DLS) optogenetics. **(F-G)** 20Hz stimulation of D1-SPNs in DLS facilitates locomotion (F, n = 5, unpaired two-tailed t-test, t = 4.736, P = 0.0003), while stimulation of D2-SPNs in DLS does not significantly suppress locomotion in open field (G, n = 5, unpaired two-tailed t-test, t = 1.026, P = 0.3224). ***, P < 0.001. **(H)** Schematic of rabies-ChR2 labeling of the inputs to D1 or D2-SPNs and optogenetic stimulation in MCC. **(I-J)** 20Hz stimulation of MCC neurons projecting to D1-SPNs facilitates locomotion (I, n = 9, unpaired two-tailed t-test, t = 2.344, P = 0.0344), while stimulation of MCC neurons projecting to D2-SPNs does not alter locomotion (J, n = 10, unpaired two-tailed t-test, t = 1.214, P = 0.2447). *, P < 0.05. **(K)** Schematic of rabies-ChR2 labeling of the inputs to D1 or D2-SPNs and optogenetic stimulation in M1. **(L-M)** 20Hz stimulation of the M1 neurons projecting to D1-SPNs facilitates locomotion (L, n = 7, Unpaired two-tailed t-test, t = 3.276, P = 0.0055), while stimulation of the M1 neurons projecting to D2-SPNs does not significantly alter locomotion (M, n = 8, Unpaired two-tailed t-test, t = 0.5796, P = 0.5714). **, P < 0.01. **(N)** Schematic of a mouse performing intracranial self-stimulation (ICSS) behavior. **(O-P)** D1-SPN (red) but not D2-SPN stimulation (black) drives ICSS behavior in both the DMS (O: D1, n = 6, permutation test, slope = 1.5060, P = 0.0378; D2, n = 5, permutation test, slope = -0.2214, P = 0.1021; one-tailed Mann Whitney test, Day 7 D1 vs. D2, P = 0.0130) and the DLS (P: D1, n = 6, permutation test, slope = 28.1429, P = 0.0082; D2, n = 5, permutation test, slope = -0.3429, P = 0.0463; one-tailed Mann Whitney test, Day 7 D1 vs. D2, P = 0.0390). *, P < 0.05. **(Q)** Timeline of helper virus injections, rabies-ChR2 injections and optogenetic stimulation for ICSS behavior. **(R-S)** Optogenetic stimulation of the cortical neurons projecting to either D1- or D2-SPNs induces ICSS behavior in both the MCC (R: MCC-D1, n = 5, permutation test, Day1-Day7, slope = 2.5857, P = 0.0034; MCC-D2, n = 5, Day2-Day7, permutation test, slope = 1.4229, P = 0.0344; no significant effect on Day7, MCC-D1 vs. MCC-D2, two-tailed Mann Whitney test, P = 0.9999) and the M1 (S: M1-D1, n = 5, permutation test, Day1-Day7, slope = 1.8214, P = 0.0259; M1-D2, n = 5, Day1-Day7, permutation test, slope = 1.8214, P = 0.0025; no significant effect on Day7, M1-D1 vs. M1-D2, two-tailed Mann Whitney test, P = 0.3810). n.s., not statistically significant.

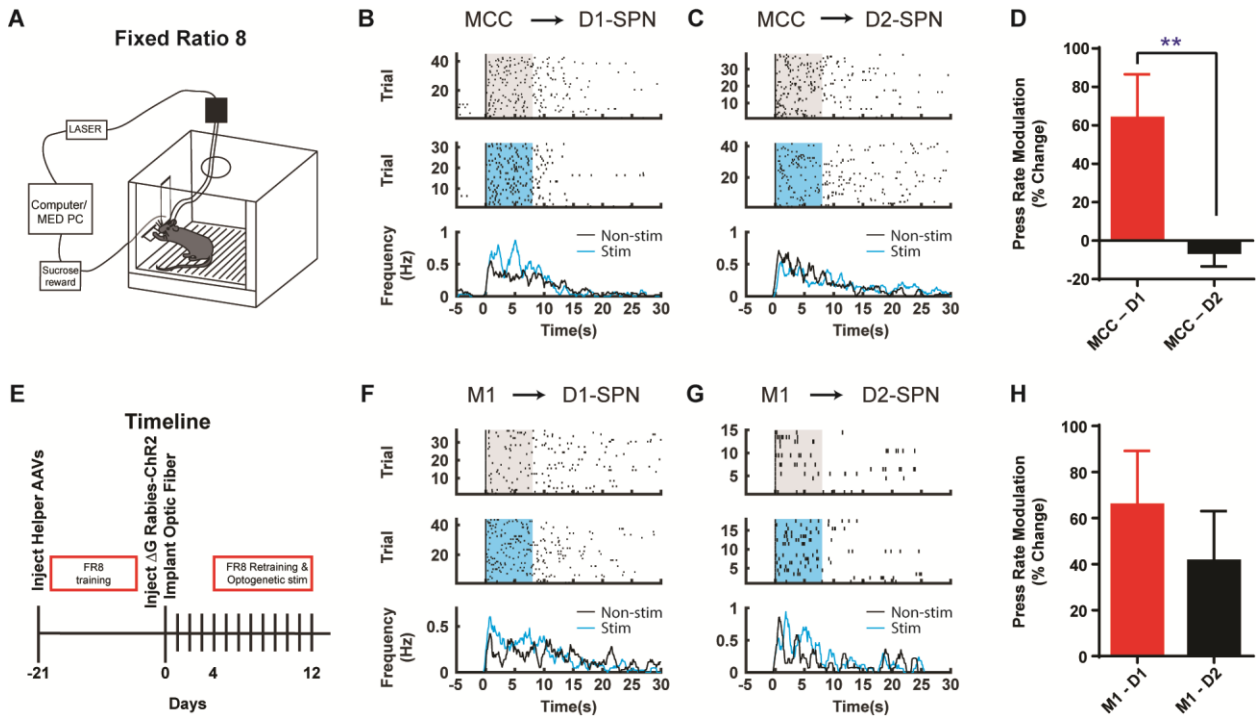

Figure 4. Optogenetic stimulation of D1- vs. D2-SPN projecting cortical neurons differently modulates action sequence execution. (A) Schematic of a mouse performing FR8 sequence. **(B)** Optogenetic stimulation (20Hz) of the D1-SPN projecting MCC neurons during FR8 sequence. Example lever pressing (black bar) in control (top) vs. stimulation (middle) trials aligned to the first press, where the blue transparent rectangle corresponds to the window of optogenetic stimulation (20Hz, 8s). The black and blue lines in the PETH (bottom) indicate the lever press rate for control and stimulation conditions, respectively, same for below. **(C)** Optogenetic stimulation (20Hz) of the D2-SPN projecting MCC neurons during FR8 sequence. **(D)** Average percent lever press rate change during optogenetic stimulation of D1- vs. D2-SPN projecting MCC neurons compared to control (MCC – D1, $n = 8$; MCC – D2, $n = 7$; Unpaired two-tailed t-test, $t = 2.774$, $P = 0.0097$). **, $P < 0.01$. Effects compared to a theoretical percentage change of 0 of each individual manipulation (MCC-D1, $n = 8$, one-sample two-tailed t-test, $t = 2.814$, $P = 0.0131$; MCC-D2, $n = 7$, one-sample two-tailed t-test, $t = 0.8481$, $P = 0.4117$). **(E)** Timeline of helper virus injections, rabies-ChR2 injections and optogenetic stimulation during action sequence performance. **(F-G)** Optogenetic stimulation (20Hz) of the D1- (F) or D2-SPN (G) projecting M1 neurons during FR8 sequence. **(H)** Average percent lever press rate change during optogenetic stimulation of D1- vs. D2-SPN projecting M1 neurons compared to control (M1 – D1, $n = 6$; M1 – D2, $n = 7$; Unpaired two-tailed t-test, $t = 0.7651$, $P = 0.4511$). Effects compared to a theoretical percentage change of 0 of each individual manipulation (M1-D1, $n = 6$, one-sample two-tailed Wilcoxon signed-rank test, $P = 0.0046$; M1-D2, $n = 7$, one-sample two-tailed Wilcoxon signed-rank test, $P = 0.0479$).

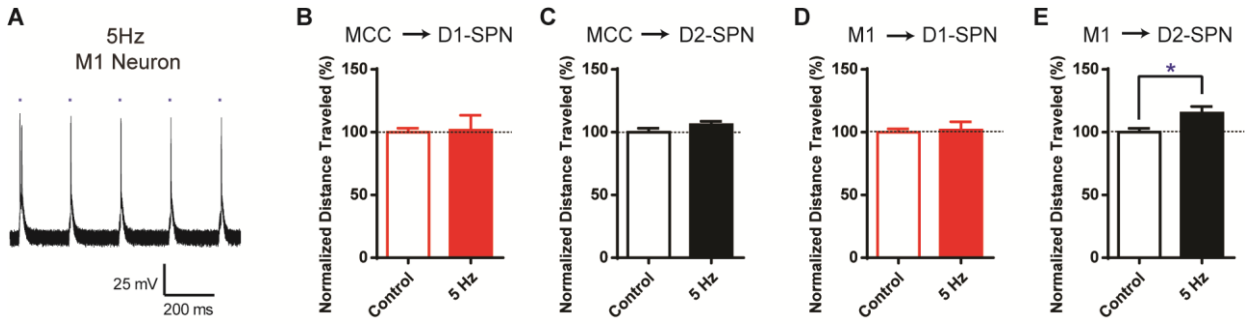

Figure S1. Low-frequency (5 Hz) optogenetic stimulation of cortical neurons projecting to striatal D1- or D2-SPNs has little effect on locomotion activity. (A) 5 Hz optogenetic stimulation elicits action potentials with high fidelity in a ChR2-mCherry positive M1 pyramidal neuron in layer 5 projecting to striatal D1-SPNs. Scale bars, 200 ms, 25 mV. **(B-C)** 5 Hz optogenetic stimulation on MCC neurons projecting to either D1- or D2-SPNs didn't change the locomotion activity. MCC – D1, $n = 9$, unpaired two-tailed t-test, $t = 0.1906$, $P = 0.8516$. MCC – D2, $n = 10$, unpaired two-tailed t-test, $t = 1.015$, $P = 0.3275$. **(D)** 5 Hz optogenetic stimulation of M1 neurons projecting to D1-SPNs didn't change the locomotion activity. $n = 7$, unpaired two-tailed t-test, $t = 0.276$, $P = 0.7866$. **(E)** 5 Hz optogenetic stimulation of M1 neurons projecting to D2-SPNs slightly increased locomotion activity. $n = 8$, unpaired two-tailed t-test, $t = 2.48$, $P = 0.0265$. *, $P < 0.05$.

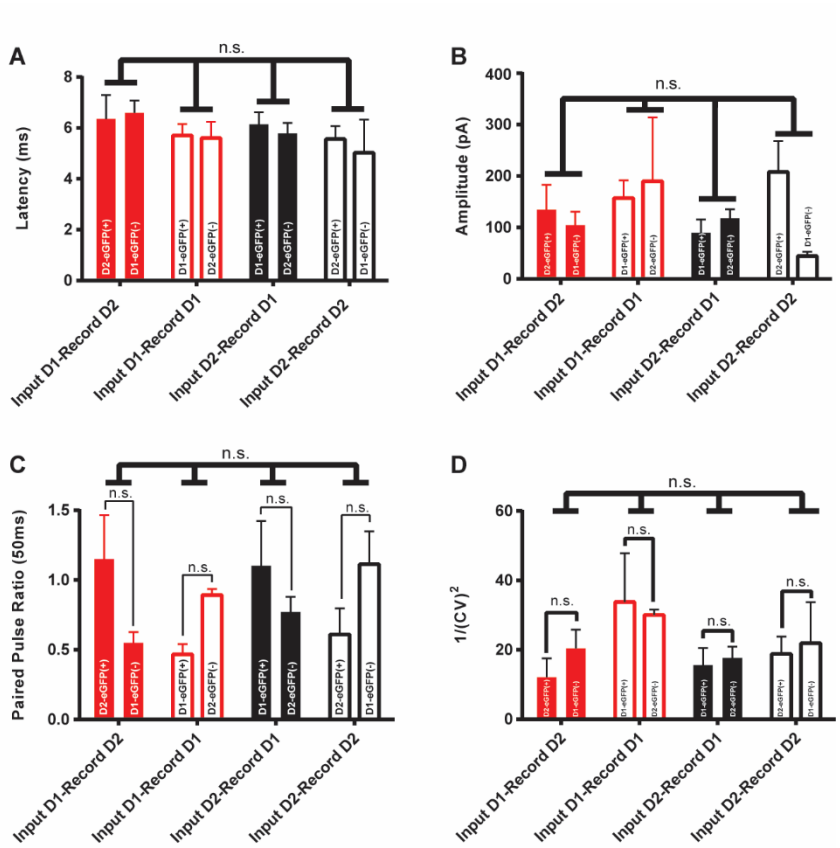

Figure S2. The synaptic properties of projections from D1- or D2-SPN retrogradely-labeled cortical inputs to striatal D1- or D2-SPNs. (A-D) The EPSC latency (A), amplitudes (B), paired pulse ratio (C) and variation (D) of whole-cell recordings of rabies-negative striatal D1- or D2-SPNs, with optogenetic stimulation of the terminals of D1- or D2-SPN retrogradely-labeled cortical neurons. n.s., $P > 0.05$, not statistically significant.

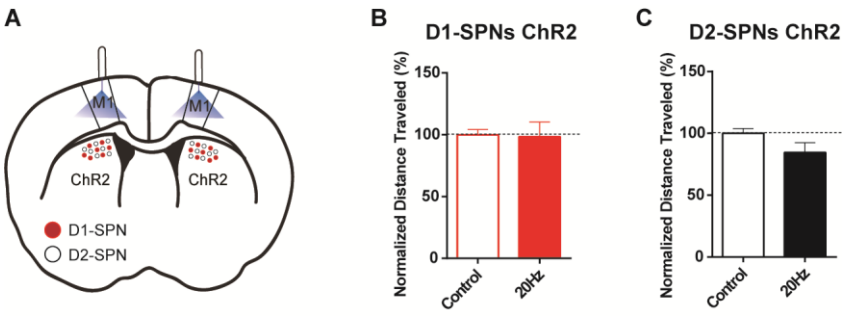

Figure S3. No effects of optogenetic stimulation of M1 on locomotion in mice with ChR2 expression in either D1- or D2-SPNs of DMS. (A) Schematic of dorsal medial striatum (DMS) injection of Cre-dependent AAV-ChR2 in D1- and A2a-Cre mice with optogenetic simulation in M1. **(B)** 20Hz optogenetic stimulation of M1 in mice expressing ChR2 in striatal D1-SPNs didn't change the locomotion activity. $n = 5$, unpaired two-tailed t-test, $t = 0.1016$, $P = 0.9194$. **(C)** 20Hz optogenetic stimulation of M1 in mice expressing ChR2 in striatal D2-SPNs didn't alter the locomotion activity. $n = 5$, unpaired two-tailed t-test, $t = 1.155$, $P = 0.2525$.